Eur Radiol (2012) 22:559–568
DOI 10.1007/s00330-011-2279-z

CARDIAC

Cardiac MRI: evaluation of phonocardiogram-gated cine imaging for the assessment of global und regional left ventricular function in clinical routine

Kai Nassenstein · Stephan Orzada · Lars Haering · Andreas Czylwik · Michael Zenge · Holger Eberle · Thomas Schlosser · Oliver Bruder · Edgar Müller · Mark E. Ladd · Stefan Maderwald

Received: 10 July 2011 / Revised: 30 August 2011 / Accepted: 6 September 2011 / Published online: 24 September 2011

Abstract
Objectives To validate a phonocardiogram (PCG)-gated cine imaging approach for the assessment of left ventricular (LV) function.
Methods In this prospective study, cine MR imaging of the LV was performed twice in 79 patients by using retrospectively PCG- and retrospectively ECG-gated cine SSFP sequences at 1.5 T. End-diastolic volumes (EDV), end-systolic volumes (ESV), stroke volumes (SV), ejection fraction (EF), muscle mass (MM), as well as regional wall motion were assessed. Subgroup analyses were performed for patients with valvular defects and for patients with dysrhythmia.
Results PCG-gated imaging was feasible in 75 (95%) patients, ECG-gating in all patients. Excellent correlations were observed for all volumetric parameters ($r>0.98$ for all variables analysed). No significant differences were observed for EDV (−0.24±3.14 mL, $P=0.5133$), ESV (−0.04±2.36 mL, $P=0.8951$), SV (−0.20±3.41 mL, $P=0.6083$), EF (−0.16±1.98%, $P=0.4910$), or MM (0.31±4.2 g, $P=0.7067$) for the entire study cohort, nor for either of the subgroups. PCG- and ECG-gated cine imaging revealed similar results for regional wall motion analyses (115 vs. 119 segments with wall motion abnormalities, $P=0.3652$).
Conclusion The present study demonstrates that PCG-gated cine imaging enables accurate assessment of global and regional LV function in the vast majority of patients in clinical routine.
Key Points
- *Phonocardiogram-gating is an alternative to electrocardiographic-gating in cardiac MR.*
- *Phonocardiogram-gated imaging allows reliable assessment of global and regional left-ventricular function.*
- *Phonocardiogram-gating is feasible in patients with valvular lesions or cardiac dysrhythmia.*
- *Because phonocardiogram-gating is insensitive to magneto-hydrodynamic effects, it is suitable for ultra-high field.*

Keywords Cardiac magnetic resonance imaging · Cine imaging · ECG gating · PCG gating · Left ventricular function

K. Nassenstein (✉) · T. Schlosser · M. E. Ladd · S. Maderwald
Department of Diagnostic and Interventional Radiology and Neuroradiology, University Hospital Essen, Hufelandstrasse 55,
45122 Essen, Germany
e-mail: Kai.Nassenstein@uni-due.de

S. Orzada · M. E. Ladd · S. Maderwald
Erwin L. Hahn Institute for Magnetic Resonance Imaging, University Duisburg-Essen,
Essen, Germany

L. Haering · A. Czylwik
Department of Communication Systems, University Duisburg-Essen,
Duisburg, Germany

M. Zenge · E. Müller
Siemens Healthcare,
Erlangen, Germany

H. Eberle · O. Bruder
Department of Cardiology and Angiology, Elisabeth Hospital Essen,
Essen, Germany

Introduction

Within the last decade, cardiac magnetic resonance imaging (CMR) has emerged as the accepted gold standard for the assessment of global and regional left ventricular (LV) functions since it enables highly accurate and reproducible quantification of LV volumes and muscle mass independent from geometric assumptions [1, 2]. Since data acquisition in magnetic resonance imaging (MRI) is inherently relatively slow and a high spatial and temporal resolution is mandatory for sufficient assessment of LV function, *k*-space lines are commonly acquired over several heartbeats to facilitate CMR with high spatiotemporal resolution [3]. Therefore, for image reconstruction a synchronisation of the acquired *k*-space lines to the cardiac cycle is obligatory. Commonly, electrocardiographic (ECG) triggering techniques are used in clinical routine to synchronise data acquisition to the cardiac cycle, whereby the R-wave, as the highest spike, is detected as the trigger pulse [4].

Because of the flow of blood, which has significant electrical conductivity, through the magnetic field, the electrocardiogram signal is altered during MRI (so-called "magneto-hydrodynamic effects") [5]. In particular, the T-wave is elevated because aortic flow is greatest during the occurrence of the T-wave [5]. At lower field strengths ($\leq$ 1.5 T) this artificial modification of the ECG trace does not hamper adequate ECG triggering in the vast majority of cases in clinical routine. Since the artificial modification of the ECG increases with increasing field strengths [6], ECG triggering fails at ultra-high field strength (e.g. 7 T) in a large number of cases due to misinterpretation of elevated T-waves as R-waves [7].

Commercially available pulse wave triggering via finger pulse oximetry is available as an alternative. However, pulse wave triggering is in principle limited by the physiologically more rounded profile of the pulse wave, which leads to less precise triggering and, consequently, to cardiac motion artefacts in the form of blurry cine images. Almost two decades ago, acoustic monitoring of both heart and respiratory sounds was investigated to ensure MR compatibility and safety [8], and recently this auscultatory approach has been described for acoustic triggering using the first heart tone as a trigger impulse for cardiac imaging [7]. The principal advantages of this triggering approach are its intrinsic insensitivity to magneto-hydrodynamic effects and its use of a well-defined trigger impulse—the first heart tone. So far, this triggering approach for cine imaging of the LV had only been evaluated in a rather small number of healthy volunteers [9]. Therefore, our study aimed to validate the diagnostic accuracy of acoustic triggered cine imaging for the assessment of LV global and regional functions in clinical routine at 1.5 T.

Materials and methods

The study was approved by the local ethics committee, and written informed consent was obtained from all patients prior to CMR. Over a 6-week period, all patients who were referred to our department for CMR and who were willing to participate in the study were enrolled, resulting in a total of 79 patients (53 men and 26 women; mean age 60.5± 15.3 years, range 18 to 89 years). Indications for CMR were: known or suspected coronary heart disease (n=53), suspected myocarditis (n=11), valvular heart disease (n=4), and various cardiomyopathies (n=11). Mitral vale replacement with implantation of a 29-mm Regent™ valve (St. Jude Medical, St. Paul, MN, USA) had been performed in one patient of the study population (Fig. 1).

Phonocardiogram (PCG) gating

For acoustic triggering, an in-house developed PCG gating device was used (Fig. 2). The stethoscope was composed of an optoacoustic microphone (Optimic 4135S, Optoacoustics, Haifa, Israel) containing no conductive parts. The acoustic signal was therefore directly converted to an optical signal at the subject and could be fed interference-free to the real-time processing system. For real-time signal processing, a digital signal processing (DSP) card (DS1104, dSpace, Germany) was integrated via a PCI (Peripheral Component Interconnect) slot into a normal Windows™ (Microsoft, Redmond, Washington, USA) personal computer. For signal detection, signal processing, and trigger generation, a Simulink model (Matlab toolbox, The Mathworks, Natick, MA, USA) was compiled to C code to drive the DSP card. The acquired heart sound was sampled with a sampling rate of 3 kHz.

For auscultation of the heart tones, the microphone was in principle placed at the left sternal border toward the apex of the heart on top of or beneath the patients' clothes. However, the exact placement of the microphone was influenced by the individual patient's anatomy, since it had to be ensured that the microphone was in close contact to the chest during the entire MRI. To minimise displacement of the microphone during MRI, the microphone was fixed to the chest with an elastic strap.

To extract the first heart tone (S_1) from the other heart tones and the acoustic noise generated e.g. by the patients themselves, the coldheads of the magnet, and by the MR gradient system during sequence acquisition, a self-developed filtering algorithm was used, which was primarily based on a finite impulse response (FIR) Hamming filter for low-pass filtering. After low-pass filtering, a threshold-based algorithm was used to differentiate the first heart tone (S_1) from the second (S_2) based on the physiological fact that S_1 has a higher amplitude/is louder than S_2.

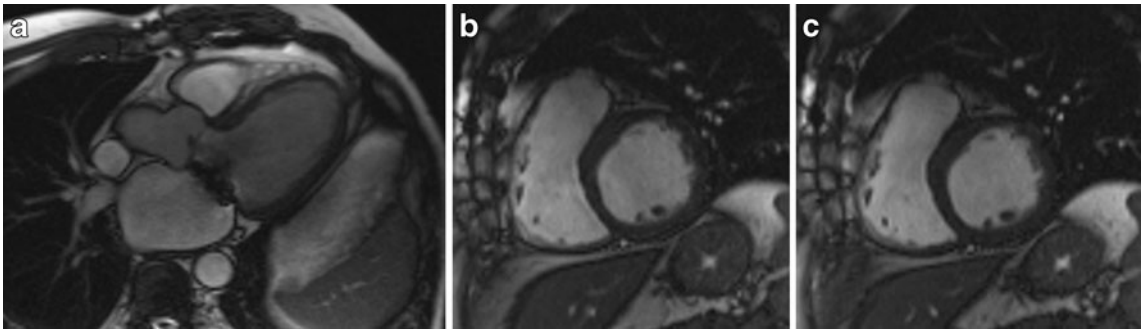

Fig. 1 ECG (**a**, **b**) and PCG (**c**) gated cine images of a 65-year-old male patient with suspected coronary heart disease and mitral valve replacement showing similar image quality of the ECG- and PCG-gated cine SSFP images

After the detection of the S_1 tone, a transistor–transistor (TTL) logic signal was generated by the DSP card as a trigger pulse. This trigger signal was directly fed via bayonet Neill–Concelman (BNC) cable into the external trigger input of the MR system's physiological measurement unit (PMU). Consequently, both ECG and PCG could be acquired simultaneously.

Image acquisition

MR examinations were performed at 1.5 T (Magnetom Avanto, Siemens Healthcare, Erlangen, Germany) equipped with high-performance gradients (SQ-Engine: maximum amplitude 45 mT/m, slew rate 200 mT/m/ms). For image acquisition, two elements of the body matrix coil and a phased-array torso coil with six active coil elements (Tim Body Matrix coil, Siemens Healthcare, Erlangen, Germany) were used.

Cine imaging of the LV was performed twice by acquiring a retrospectively PCG as well as retrospectively ECG-gated, generalised autocalibrating partially parallel acquisition (GRAPPA) accelerated, steady-state free precession sequence in standard short-axis orientation during breath-hold at end expiration: TR 2.63 ms, TE 1.12 ms, FA 72°, field of view (FOV) 270×203 mm^2–360×270 mm^2 depending on the anatomy of the individual patient, matrix 192×144 (resulting in spatial in-plane resolution of 1.4×1.4 mm^2–1.9×1.9 mm^2), acquisition of 15*k*-space lines per segment resulting in a temporal resolution of 39.45 ms, 25 calculated phases, bandwidth 930 Hz/pixel, slice thickness 8 mm, no interslice gap, number of acquired slices 9–16, acceleration factor 2. The two datasets were acquired in randomised order. The acquisition times were recorded for each short-axis cine sequence. Additionally, the mean heart rates during image acquisition were recorded for both gating approaches in each individual.

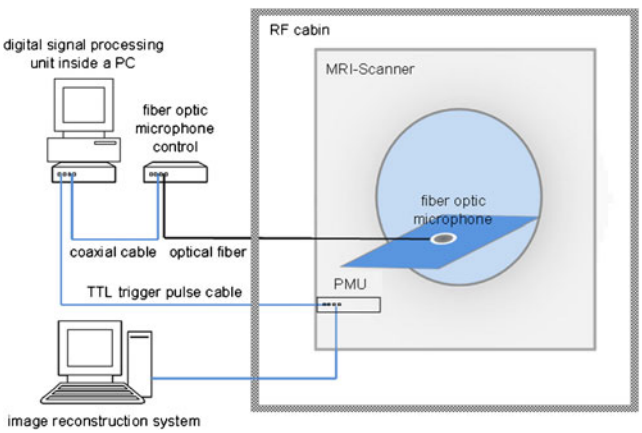

Fig. 2 Schematic description of the phonocardiogram (PCG) gating device and its connection to the MRI system

Image analysis

The datasets were evaluated by one experienced observer (>3000 evaluated CMR examinations) in randomised order blinded to the results of the analysis of the corresponding dataset.

Calculations of the LV volumes and the LV mass were performed using the ARGUS™ software (Siemens Healthcare, Erlangen, Germany), which provides semiautomatic contour detection. Manual correction of the automatically rendered endo- and epicardial contours was performed in all cases. Papillary muscles as well as myocardial trabeculations were included into the ventricular cavity. End-diastole (ED) was defined visually as the phase of the cardiac cycle with the largest left ventricular cavity at mid-ventricle, and end-systole (ES) as the phase with smallest LV cavity. At the base of the heart, slices were considered to be in the LV if the blood was surrounded by ventricular myocardium over at least 270°. The apical slice was defined as the last slice showing intra-cavity blood pool.

Regional wall motion was evaluated visually and characterised as normal, hypo-, a- or dyskinetic for all cardiac segments according to the American Heart Association (AHA) segmental model for 16 segments in short-axis orientation [10].

Gating artefacts were evaluated visually based on binary assessment (presence vs. absence of gating artefacts). From this evaluation, the percentage of short-axis scans with gating artefacts was calculated for both approaches.

Statistical analysis

Statistical analysis was performed using MedCalc Version 11.4.2.0 (MedCalc Software, Mariakerke, Belgium). Parameters were given as mean ± standard deviation or as frequency. Coefficients of variation and intraclass correlation coefficients were calculated, and the agreement between the methods was illustrated in Bland–Altman plots [11] and Passing–Bablok regression charts [12]. A two-tailed *t*-test for dependent samples was used to test for significant differences between the assessed volumetric data, the MR data acquisition times, the mean heart rates, and the observed percentages of scans with gating artefacts. A Wilcoxon test was used to test for significant differences in the observed numbers of segments with wall motion abnormalities. A chi-square test or a two-tailed *t*-test for independent samples was used to analyse differences in the physiological and pathological characteristics of patient subgroups. A *P*-value less than 0.05 was considered statistically significant. Statistical analyses were performed for the entire study cohort as well as for the subgroup of patients with valvular pathologies and for the subgroup of patients with cardiac dysrhythmia.

Results

PCG-gated cine imaging was feasible in 75 of 79 (95%) patients and ECG-gated imaging in all patients (100%). In 4 patients (2 women, 2 men; mean age 56.8±20.4 years, range 39 to 86 years; mean BMI 28.6±4.0 kg/m^2, range 26.1 to 34.6 kg/m^2; valve lesions 1/4; arrhythmia 1/4) PCG gating failed. The mean heart rate was 74.1±14.1 beats per minute (range 55 to 125 bpm) during ECG-gated data acquisition and 73.9±11.9 beats per minute (range 54 to 118 bpm) during PCG-gated acquisition (P=0.8773). The mean short-axis MR data acquisition time was 5.86± 3.82 s for ECG-gated image acquisition and 5.83±2.83 s for PCG-gated acquisition (P=0.9572).

Results of LV volume and global functional measurements for the entire study cohort are summarised in Table 1. No significant differences were observed between end-diastolic volumes (EDV), end-systolic volumes (ESV), stroke volumes (SV), left ventricular ejection fractions (EF), or left ventricular muscle mass (MM) derived from the two gating approaches (Table 1). Volumetric data derived from the PCG-gated imaging approach showed excellent correlation with the volumetric data from the

Table 1 Left ventricular volumes and mass as assessed with ECG- or PCG-gated cine SSFP imaging for the entire study cohort (n=75)

	ECG-gated cine SSFP		PCG-gated cine SSFP		Difference		*t*-test *P*	Intraclass correlation coefficient
	Mean ± SD	CV	Mean ± SD	CV	Mean ± SD	95% CI for the mean		
EDV	129.8±39.1 mL	0.302	129.5±39.5 mL	0.305	−0.24±3.14 mL	−0.96 to 0.49 mL	0.5133	0.9968
ESV	50.7±33.6 mL	0.663	50.6±34.0 mL	0.671	−0.04±2.36 mL	−0.58 to 0.51 mL	0.8951	0.9976
SV	79.1±21.5 mL	0.271	78.9±22.2 mL	0.281	−0.20±3.41 mL	−0.99 to 0.58 mL	0.6083	0.9880
EF	62.9±13.1%	0.208	62.7±13.3%	0.212	−0.16±1.98%	−0.61 to 0.30%	0.4910	0.9888
MM	127. 1±33.3 g	0.262	127.7±33.9 g	0.266	0.53±4.08 g	−0.41 to 1.47 g	0.2645	0.9926

EDV end-diastolic volume, *ESV* end-systolic volume, *SV* stroke volume, *EF* ejection fraction, *MM* muscle mass, *SD* standard deviation, *CV* coefficient of variation, *CI* confidence interval

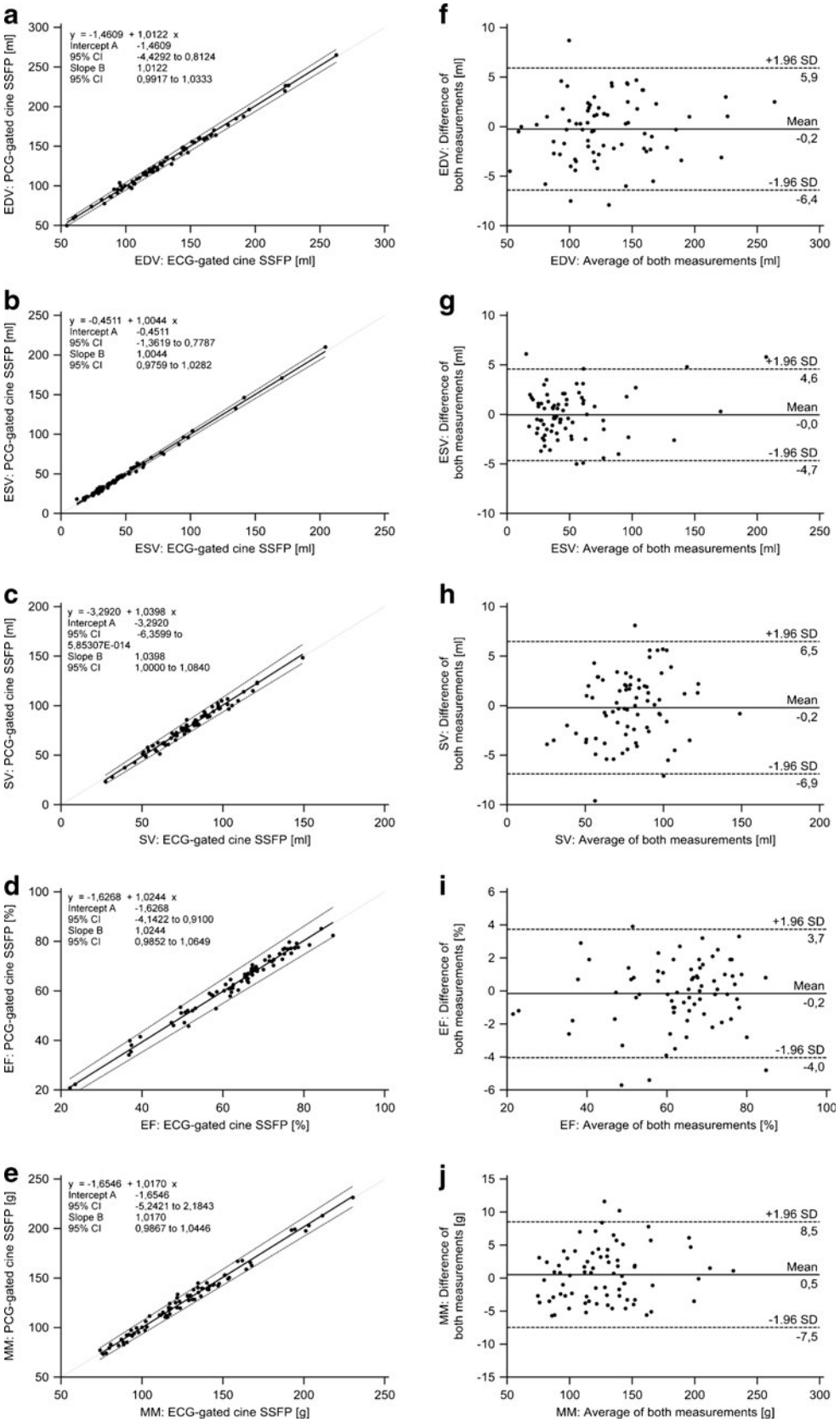

Fig. 3 Passing–Bablok regression charts (**a**–**e**) and Bland-Altman analyses (**f**–**j**) depict the agreement between the volumetric parameters derived from the ECG- and PCG-gated cine SSFP datasets, revealing no systematic differences

standard ECG-gated cine imaging approach for all variables analysed as demonstrated in the Passing–Bablok regression charts (Figs. 3a–e). Bland–Altman plots demonstrated excellent agreement between the results derived from both

Table 2 Results of visual wall motion assessment for the entire study cohort (n=75)

	Number of				Total number of segments with wall motion abnormalities
	Normokinetic segments	Hypokinetic segments	Akinetic segments	Dyskinetic segments	
ECG-gated cine SSFP	1081	89	25	5	119
PCG-gated cine SSFP	1085	84	27	4	115

gating approaches (Figs. 3f–j). Regional wall motion abnormalities were observed in 34 patients in a total of 119 segments when evaluating the ECG-gated datasets, and in 33 patients in a total of 115 segments (P=0.3652) when evaluating the PCG-gated datasets (Table 2). Evaluation of the short-axis sequences for gating artefacts per patient revealed a mean percentage of cine short-axis images with gating artefacts of 8.78±13.38% (range 0% to 47%) for the ECG-gating approach and of 13.85±17.79% (range 0% to 70%) for the PCG-gating approach (P=0.0059); however, in the majority of cases excellent image quality was observed with both gating approaches (Fig. 4). To guarantee diagnostic quality of each dataset, 30 ECG-gated short-axis sequences and 36 PCG-gated short-axis sequences (P=0.4832) had to be repeated (Fig. 5). Physiological and pathological characteristics of patients with gating artefacts in the cine SSFP datasets and of patients in whom repetition of cine slices had been necessary are given in Table 3.

Twenty-eight of our 79 patients (35.4%) showed valvular lesions in CMR (mitral valve incompetence in 21, tricuspid valve incompetence in 9, aortic valve incompetence in 8, and aortic valve stenosis in 5 patients, while 15 patients showed one, 11 patients a combination of two, and 2 patients a combination of three of these valve defects). In this subgroup, PCG gating was feasible in 27 patients (96.4%); only in one patient with severe aortic valve stenosis did PCG gating fail. As summarised in Table 4, no significant differences were observed between the volumetric data derived from both gating approaches, and excellent correlations between both gating approaches was observed for all variables analysed. Similar to the results for the entire study cohort, a trend toward a higher percentage of images with gating artefacts was observed for the PCG-gating approach compared to the ECG-gating approach (15.5% vs. 10.2%, P=0.0975).

Fourteen of our 79 patients (16.5%) had cardiac dysrhythmia (11 patients with ectopic heart beats, 3 patients with atrial fibrillation) at the time of CMR. In this subgroup PCG gating was feasible in 13 patients (93%). For this subgroup no significant differences were observed between the volumetric data derived from both gating approaches, and excellent correlations between both gating approaches were observed for all variables analysed (Table 5). Gating artefacts were observed in 27.5% of these ECG-gated cine short-axis images and in 34.8% of the PCG-gated images (P=0.2054).

Discussion

To facilitate high spatiotemporal resolution of CMR, it is currently necessary to acquire k-space lines over several heartbeats, which necessitates a reliable correlation of the acquired k-space lines to the cardiac cycle for image reconstruction. The current standard technique for this synchronisation is based on simultaneous ECG recording

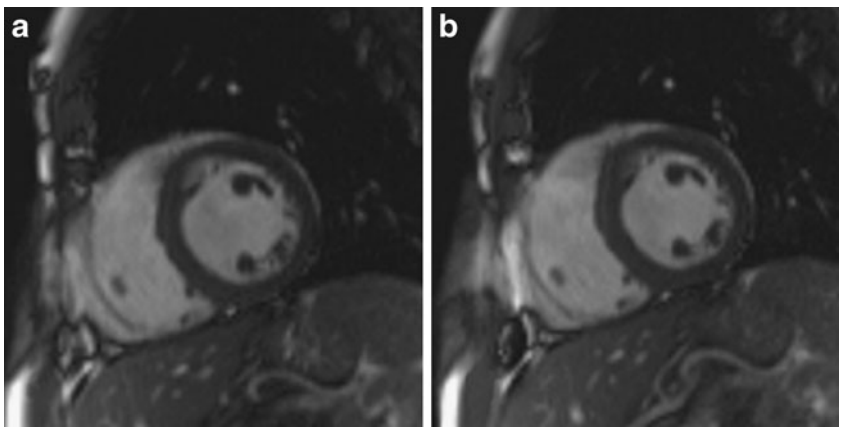

Fig. 4 Mid-ventricular short-axis cine SSFP scans of a 51-year-old male patient with suspected coronary heart disease acquired with ECG (**a**) and PCG (**b**) gating: visually comparable image quality of both gating approaches

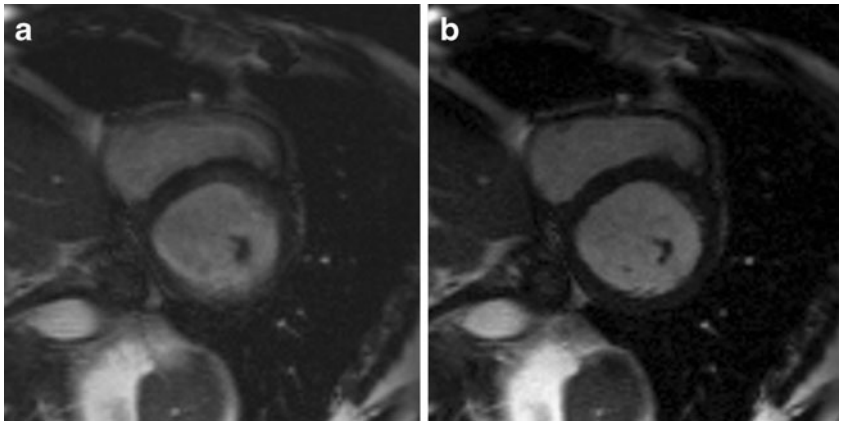

Fig. 5 Mid-ventricular short-axis cine SSFP MR images of a 60-year-old male patient with suspected coronary heart disease acquired twice with PCG gating: whereas the initial acquired image (**a**) shows gating artefacts particularly at the lateral wall of the left ventricle, the repeated image (**b**) shows a good image quality without gating artefacts

during data acquisition ("ECG gating"/"ECG triggering"). Since CMR, similar to other applications of clinical MRI, is moving towards imaging at higher field strengths, the question of how to synchronise data acquisition to the cardiac cycle again becomes relevant, since artificial modification of the ECG trace increases with increasing field strengths due to magneto-hydrodynamic effects. Phonocardiogram (PCG) gating has recently been introduced for CMR [7]. Since this approach had not been validated in patients so far, our study aimed to validate PCG-gated cine imaging for the assessment of global and regional LV function in a non-selected patient population in clinical routine.

Our study demonstrates for the first time that PCG-gated cine imaging allows reliable assessment of global and regional LV function in the vast majority of patients in clinical routine. Moreover, our results indicate that even in patients with valve pathologies, PCG-gated cine imaging is feasible and on a par with ECG-gated imaging. This is important, since it demonstrates that the post-processing algorithm utilised here is feasible to generate a reliable trigger even in the presence of pathological heart murmur. Furthermore, in one patient with valve replacement our data indicates that PCG gating is also feasible, and our study showed that PCG-gated triggering is robust against cardiac dysrhythmia, which in fact is not surprising since the post-processing algorithm is not based on the detection of rhythm within the raw data.

Although we observed excellent agreement between ECG- and PCG-gated cine imaging for the assessment of global and regional LV function, it must be noted that this excellent agreement only applies to retrospectively gated cine imaging. Since the heart tone S_1, which is caused by the sudden block of reverse blood flow due to closure of the atrioventricular valves at the beginning of ventricular contraction, occurs at the end of the QRS complex, an imminent delay between the physiological signals used for PCG and ECG gating exists. Moreover, since the post processing of the acoustic raw data requires additional time, the PCG-generated trigger signal currently has an additional delay [13]. Even though not demonstrated in our study, this delay would presumably bias the assessment of global LV function when using prospectively triggered cine sequences due to the fact that the beginning of systole would be not included in the cine images.

Despite the excellent agreement between PCG- and ECG-gated assessment of global and regional LV function, it must be noted that in 4 of our 79 (5%) patients PCG gating failed. When looking at the characteristics of the patients in whom PCG gating failed, no common physiological (sex, age, body-mass-index) or pathological (valve pathology, cardiac dysrhythmia) feature could be found. Therefore, an external, patient independent effect seems to have caused failure of PCG gating in the 4 patients. A possible, even though speculative, reason for failure of PCG gating might have been a shift of the microphone during movement of the patient into the isocenter of the magnet, which might have led to insufficient recording of the heart tones. Moreover, when looking at the visual image quality assessment, it must be noted that we observed a higher frequency of cine images with gating artefacts for the PCG gating approach. Since gating artefacts are caused by a misinterpretation of background noise as heart tones, further refinements of the post-processing algorithm (e.g. implementation of additional filtering algorithms) are necessary to improve the robustness of the triggering software. However, it must be emphasised that the higher frequency of gating artefacts in the PCG-gated cine imaging datasets had no statistically adverse effects on the assessment of global and regional LV function in our study.

Analysis of the physiological and pathological characteristics of the patients with gating artefacts in the ECG- or PCG-gated cine datasets and of patients in whom repetition of cine slices had been necessary, revealed only a significant higher frequency of dysrhythmia in case of ECG gating, whereas no

Table 3 Physiological and pathological characteristics of patients with gating artefacts in the cine SSFP datasets and of patients in whom it had been necessary to repeat cine slices to ensure diagnostic quality of the cine datasets

	Entire study cohort	Gating artefacts in				Repeated slices in			
		ECG-gated datasets		PCG-gated datasets		ECG-gated datasets		PCG-gated datasets	
			P		*P*		*P*		*P*
n	79	30	–	45	–	16	–	17	–
Sex (f/m)	26/53	11/19	0.8860	14/31	0.9949	7/9	0.5875	6/11	0.9247
Age [years]	60.5±15.3	61.3±16.8	0.7976	60.9±15.5	0.8896	59.9±20.7	0.9056	59.8±18.9	0.8802
Body-mass-index [kg/m^2]	26.4±3.8	25.8±4.3	0.4931	26.4±4.1	0.9930	25.4±3.9	0.3388	26.5±4.0	0.9173
Valvular pathologies [%]	35.4	33.3	0.9852	33.3	0.9672	35.3	0.7888	50.0	0.3796
Dysrhythmia [%]	16.5	40.0	0.0288	26.7	0.3435	52.9	0.0056	38.9	0.0988
Heart rate [bpm]	74.1±14.1	72.4±10.5	0.5651	71.7±8.6	0.3082	82.5±16.5	0.0610	80.2±13.3	0.0789

Table 4 Left ventricular volumes and mass as assessed with ECG- or PCG-gated cine SSFP imaging for the subgroup of patients with valve pathologies (n=27)

	ECG-gated cine SSFP		PCG-gated cine SSFP		Difference		*t*-test *P*	Intraclass correlation coefficient
	Mean ± SD	CV	Mean ± SD	CV	Mean ± SD	95% CI for the mean		
EDV	135.1±46.7 mL	0.346	135.2±46.9 mL	0.347	0.05±2.54 mL	−0.96 to 1.05 mL	0.9223	0.9986
ESV	60.2±46.1 mL	0.766	60.5±46.7 mL	0.771	0.39±2.27 mL	−0.51 to 1.29 mL	0.3814	0.9988
SV	75.0±23.2 mL	0.310	74.6±23.2 mL	0.311	−0.34±2.93 mL	−1.50 to 0.82 mL	0.5511	0.9922
EF	58.9±16.8%	0.286	58.7±17.0%	0.290	−0.24±1.87%	−0.98 to 0.50%	0.5090	0.9940
MM	133.9±36.8 g	0.275	134.2±37.4 g	0.279	0.31±4.2 g	−1.35 to 1.97 g	0.7067	0.9938

EDV end-diastolic volume, *ESV* end-systolic volume, *SV* stroke volume, *EF* ejection fraction, *MM* muscle mass, *SD* standard deviation, *CV* coefficient of variation, *CI* confidence interval

Table 5 Left ventricular volumes and mass as assessed with ECG- or PCG-gated cine SSFP imaging for the subgroup of patients with dysrhythmia ($n=13$)

	ECG-gated cine SSFP		PCG-gated cine SSFP		Difference		*t*-test *P*	Intraclass correlation coefficient
	Mean ± SD	CV	Mean ± SD	CV	Mean ± SD	95% CI for the mean		
EDV	139.7±63.5 mL	0.455	139.3±64.2 mL	0.461	−0.40±3.15 mL	−2.30 to 1.51 mL	0.6580	0.9989
ESV	79.2±59.1 mL	0.746	79.6±60.7 mL	0.762	0.44±2.85 mL	−1.28 to 2.16 mL	0.5894	0.9989
SV	60.5±17.0 mL	0.281	59.7±17.8 mL	0.299	−0.84±3.28 mL	−2.82 to 1.15 mL	0.3771	0.9825
EF	48.5±16.2%	0.333	48.0±16.8%	0.351	−0.53±2.33%	−1.94 to 0.88%	0.4300	0.9903
MM	135.7±42.4 g	0.313	135.2±45.3 g	0.335	−0.46±3.98 g	−2.87 to 1.94 g	0.6832	0.9961

EDV end-diastolic volume, *ESV* end-systolic volume, *SV* stroke volume, *EF* ejection fraction, *MM* muscle mass, *SD* standard deviation, *CV* coefficient of variation, *CI* confidence interval

significant differences were observed for the remaining physiological and pathological characteristics (sex, age, body-mass-index, valve lesions and heart rate). Since a higher frequency of gating artefacts was observed in the subgroup of patients with cardiac dysrhythmia for the ECG as well as for the PCG gating approach compared to the entire study population, also, the problem of gating artefacts in case of dysrhythmia seems to be rather the problem of cardiac imaging in presence of dysrhythmia itself than a problem of the used gating approach.

Besides its inherent insensitivity to magneto-hydrodynamic effects, which makes PCG gating attractive for imaging at higher magnetic field strengths, PCG gating has further advantages which make it interesting for CMR even at lower field strengths. First of all, the PCG gating device is very easy to use, since it is only necessary to place the microphone on the chest over the heart, whereby the microphone can even be placed on top of the patient's clothes. Therefore, time-consuming procedures like local shaving in case of chest hair in males to optimise electrode adhesion or repositioning of the ECG leads to optimise the recorded ECG trace are omitted when using the PCG triggering device. It would seem feasible to integrate the PCG microphone into a body matrix surface coil, which might improve its operator convenience further. Beyond that, since the optoacoustic microphone contains no electrically conductive parts, it features unequalled safety properties. Heating of the patient's skin and even burns which have been reported after ECG-triggered CMR [14–16], which is intrinsically an electrical measurement, are inherently excluded with the PCG device.

The present study is not without limitations. First of all, we performed only volumetric calculations, visual analyses of wall motion abnormalities, as well as binary assessment of the presence or absence of gating artefacts, and abstained from a technical analysis of PCG-gated cine imaging based on factors such as endocardial border sharpness or assessment of trigger efficiency. However, these technical analyses of PCG gating have been performed in healthy volunteers in previous studies [9, 13]. Moreover, it should be recognised that the present study aimed to assess the applicability of PCG-gated cine imaging for the assessment of global and regional LV function in clinical routine, so that clinical parameters (LV volumes, LV muscle mass, global systolic LV function and regional wall motion abnormalities) were deliberately chosen as effect variables. Since we performed only one volumetric calculation for each dataset, our study did not provide inter- or intra-observer variability. However, several previous studies have demonstrated the accuracy of the used volumetric analysis approach [17–19]. Due to the fact that datasets using each gating approach were acquired only once in each patient, the present study did not supply data for determining interstudy reproducibility.

Conclusion

In summary, the present study demonstrates that PCG-gated cine imaging enables accurate assessment of global and regional LV function in the vast majority of patients in routine clinical practice. Moreover, it has been demonstrated for the first time that acoustic triggering is even feasible in patients with valve lesions. Since PCG gating is inherently insensitive to magneto-hydrodynamic effects, this gating technique might become the method of choice for cine imaging at ultra-high magnetic field strengths. Beyond that, PCG gating might be an interesting technique even for cardiac imaging at lower field strengths due to its user-friendliness and inherent MRI safety due to lack of any electrically conducting components.

References

1. Higgins CB (1992) Which standard has the gold? J Am Coll Cardiol 19:1608–1609
2. Bellenger NG, Marcus NJ, Rajappan K, Yacoub M, Banner NR, Pennell DJ (2002) Comparison of techniques for the measurement of left ventricular function following cardiac transplantation. J Cardiovasc Magn Reson 4:255–263
3. Kramer CM, Barkhausen J, Flamm SD, Kim RJ, Nagel E (2008) Standardized cardiovascular magnetic resonance imaging (CMR) protocols, society for cardiovascular magnetic resonance: board of trustees task force on standardized protocols. J Cardiovasc Magn Reson 10:35
4. Fischer SE, Wickline SA, Lorenz CH (1999) Novel real-time R-wave detection algorithm based on the vectorcardiogram for accurate gated magnetic resonance acquisitions. Magn Reson Med 42:361–370
5. Schenck JF (2005) Physical interactions of static magnetic fields with living tissues. Prog Biophys Mol Biol 87:185–204
6. Ladd ME (2007) High-field-strength magnetic resonance: potential and limits. Top Magn Reson Imaging 18:139–152
7. Frauenrath T, Hezel F, Heinrichs U, Kozerke S, Utting JF, Kob M, Butenweg C, Boesiger P, Niendorf T (2009) Feasibility of cardiac gating free of interference with electro-magnetic fields at 1.5 Tesla, 3.0 Tesla and 7.0 Tesla using an MR-stethoscope. Invest Radiol 44:539–547
8. Henneberg S, Hok B, Wiklund L, Sjodin G (1992) Remote auscultatory patient monitoring during magnetic resonance imaging. J Clin Monit 8:37–43
9. Becker M, Frauenrath T, Hezel F, Krombach GA, Kremer U, Koppers B, Butenweg C, Goemmel A, Utting JF, Schulz-Menger J, Niendorf T (2010) Comparison of left ventricular function assessment using phonocardiogram- and electrocardiogram-triggered 2D SSFP CINE MR imaging at 1.5 T and 3.0 T. Eur Radiol 20:1344–1355
10. Cerqueira MD, Weissman NJ, Dilsizian V, Jacobs AK, Kaul S, Laskey WK, Pennell DJ, Rumberger JA, Ryan T, Verani MS (2002) Standardized myocardial segmentation and nomenclature for tomographic imaging of the heart: a statement for healthcare professionals from the Cardiac Imaging Committee of the Council on Clinical Cardiology of the American Heart Association. Circulation 105:539–542
11. Bland JM, Altman DG (1986) Statistical methods for assessing agreement between two methods of clinical measurement. Lancet 1:307–310
12. Passing H, Bablok (1983) A new biometrical procedure for testing the equality of measurements from two different analytical methods. Application of linear regression procedures for method comparison studies in clinical chemistry, Part I. J Clin Chem Clin Biochem 21:709–720
13. Frauenrath T, Hezel F, Renz W, d'Orth Tde G, Dieringer M, von Knobelsdorff-Brenkenhoff F, Prothmann M, Menger JS, Niendorf T Acoustic cardiac triggering: a practical solution for synchronization and gating of cardiovascular magnetic resonance at 7 Tesla. J Cardiovasc Magn Reson 12:67
14. Shellock FG, Kanal E (1996) Burns associated with the use of monitoring equipment during MR procedures. J Magn Reson Imaging 6:271–272
15. Kugel H, Bremer C, Puschel M, Fischbach R, Lenzen H, Tombach B, Van Aken H, Heindel W (2003) Hazardous situation in the MR bore: induction in ECG leads causes fire. Eur Radiol 13:690–694
16. Shellock FG, Crues JV (2004) MR procedures: biologic effects, safety, and patient care. Radiology 232:635–652
17. Semelka RC, Tomei E, Wagner S, Mayo J, Caputo G, O'Sullivan M, Parmley WW, Chatterjee K, Wolfe C, Higgins CB (1990) Interstudy reproducibility of dimensional and functional measurements between cine magnetic resonance studies in the morphologically abnormal left ventricle. Am Heart J 119:1367–1373
18. Moon JC, Lorenz CH, Francis JM, Smith GC, Pennell DJ (2002) Breath-hold FLASH and FISP cardiovascular MR imaging: left ventricular volume differences and reproducibility. Radiology 223:789–797
19. Heilmaier C, Nassenstein K, Nielles-Vallespin S, Zuehlsdorff, Hunold P, Barkhausen J (2010) Assessment of left ventricular function with single breath-hold highly accelerated cine MRI combined with guide-point modeling. Eur J Radiol 74:492–499